



Published in final edited form as:

Nature. 2014 July 10; 511(7508): 251–254. doi:10.1038/nature13292.

Avoidance of rNMP-induced mutations via RNaseH2 and Srs2-Exo1 dependent mechanisms

Catherine J. Potenski^{1,*}, Hengyao Niu^{2,*}, Patrick Sung^{2,3}, and Hannah L. Klein^{1,3}

¹Department of Biochemistry and Molecular Pharmacology, New York University School of Medicine, New York, NY 10016, USA

²Molecular Biophysics and Biochemistry, Yale University School of Medicine, 333 Cedar Street, New Haven, CT 06520, USA

Abstract

Srs2 helicase is known to dismantle nucleofilaments of the Rad51 recombinase to prevent spurious recombination events^{1–3, 4, 5, 6} and unwind trinucleotide sequences that are prone to hairpin formation⁷. Here we document a new, unexpected genome maintenance role of Srs2 in the suppression of mutations arising from misinsertion of rNMPs during DNA replication. In cells lacking RNaseH2, Srs2 unwinds DNA from the 5' side of a nick generated by DNA topoisomerase I⁸ at a rNMP residue. In addition, Srs2 interacts with and enhances the activity of the nuclease Exo1, to generate a DNA gap in preparation for repair. Srs2-Exo1 thus functions in a novel pathway of nick processing-gap filling that mediates tolerance of rNMPs in the genome. Our results have implications for understanding the basis of Aicardi-Goutieres Syndrome, which stems from inactivation of the human RNaseH2 complex⁹.

Mutants of *SRS2* (*hpr5*) and *RNH202* (*hpr4*), which encode a 3' to 5' helicase and a subunit of the RNaseH2 complex, respectively, are represented in our collection of hyper-rec mutants¹⁰. These mutants exhibit similar hyper-recombination levels¹⁰, DNA damage sensitivity, and interactions with DNA replication and damage repair genes (Extended Data Fig. 1). The *rnh202 srs2* double mutant was tested to determine if RNaseH2 and Srs2 might act together. A truncation mutant *srs2-860*¹ that has helicase activity but lacks Rad51 interaction was used (Fig. 1a), as we wished to distinguish between DNA helicase and Rad51 removal activities *in vivo*. We disabled the ATP hydrolysis activity of *srs2-860* through the K41A mutation (*srs2-KA860*)¹¹. The *rnh202 srs2-KA860* cells grew slowly (Fig. 1b), revealing that Srs2 helicase activity is important for growth in *rnh202*. Similar results were obtained with the *rnh201 srs2* mutant, deficient in the catalytic subunit of RNaseH2 (data not shown). We note that the *srs2-KA* mutation in the full-length protein¹¹ also engenders a slow growth phenotype with *rnh202* (Extended Data Fig. 2 a,b).

Users may view, print, copy, and download text and data-mine the content in such documents, for the purposes of academic research, subject always to the full Conditions of use:http://www.nature.com/authors/editorial_policies/license.html#terms

³To whom correspondences and requests for materials should be addressed: Patrick Sung: patrick.sung@yale.edu, Hannah Klein: Hannah.Klein@nyumc.org.

*These two authors contributed equally to this work.

Author Contributions: H.L.K. and P.S. conceived the study. C.J.P., H.N., P.S. and H.L.K. designed the experiments and analyzed the data. C.J.P. and H.N. executed the experiments and contributed equally to the work. C.J.P., H.N., P.S. and H.L.K. wrote the paper.

Cells deficient in *RNH202*, but not *SRS2*, accumulate spontaneous mutations¹⁰. Interestingly, the *rnh202 srs2* double mutant shows a much stronger mutator phenotype (Fig. 1c), indicating that *SRS2* prevents mutations in *rnh202* cells. The *srs2-860* allele possesses this mutation avoidance function, but *srs2-KA860* is defective in this regard. The *srs2-860* mutant has a hyper-rec phenotype because its encoded protein lacks anti-Rad51 activity¹, and the *rnh202 srs2-860* double mutant shows an additive increase in recombination that is partially dependent on the Srs2 helicase activity (Fig. 1d). Consistent with this finding, the *rnh202 srs2* mutant exhibits increased Rad52 foci (Extended Data Fig. 3a), indicative of spontaneous DNA double strand breaks²⁰. The slow growth phenotype of the *rnh202 srs2* mutant (Fig. 1a) is due to an increase in G2 cells and can be partially relieved by inactivating the DNA damage checkpoints (Extended Data Fig. 3b–c). Lastly, the DNA damage checkpoints are largely intact in these cells as shown by Rad53 phosphorylation following hydroxyurea (HU) treatment (Extended Data Fig. 3d), which elevates the rNTP:dNTP ratio. However, combining *rnh202* with either *srs2* or *srs2-KA860* leads to a synergistic sensitivity to HU (Fig. 1e).

Ribonucleotide misincorporation becomes elevated in cells that harbor the *pol2644G* mutation in the replicative DNA polymerase Polε²⁴, and the combination of *rnh202* with *pol2644G* increases the ribonucleotide load further²³. Importantly, the *rnh202 srs2 pol2644G* triple mutation is lethal (Fig. 1f), and the lethality is rescued by *srs2-860* but not *srs2-KA860* (data not shown).

Loss of RNaseH2 causes slippage mutations in simple repeats without affecting base substitutions^{8,23}. We sequenced *can1* alleles to determine the mutation signatures of various strains. As expected, *rnh202* cells accumulate slippage mutations, including single nucleotide deletions in a mononucleotide run and dinucleotide deletions in dinucleotide repeats (Fig. 1g, Extended Data Table 1a). The *srs2* mutant shows a slight increase in these mutation types, consistent with the role of Srs2 in preventing slippage in long trinucleotide repeats⁷. The slippage mutations are increased in the *rnh202 srs2* double mutant (Fig. 1g, Extended Data Table 1a). To further characterize this mutator phenotype, a reporter that detects slippages in AG repeats was used⁸. With this reporter, *srs2* is indistinguishable from wild type, while *rnh202* shows a 90-fold increase. This phenotype of *rnh202* is exacerbated by removing Srs2 or inactivating its helicase activity (Fig. 1h, Extended Data Fig. 2c). Altogether, the results show that Srs2 helicase guards against mutations induced by rNMPs in DNA, and they reveal an overlap in mutation sequences between *rnh202* and *rnh202 srs2* with novel slippage sites of 3 nucleotides in the double mutant (Extended Data Fig. 4, Extended Data Table 1a).

Mutations that arise in RNaseH2 deficient cells are dependent on topoisomerase I (Topo I), encoded by the *TOP1* gene, which cleaves DNA at rNMP residues^{8,26}. We tested *top1* to ask whether it is relevant for *rnh202 srs2*. Can^r mutations arise from different events, including gross chromosome rearrangements¹⁴. In our test, *top1* is epistatic to *rnh202* (Fig. 2a). Importantly, *rnh202 top1* shows a specific loss of slippage events of 2 nucleotides or greater (Fig. 2b, Extended Data Table 1a). The increased mutation rate in *rnh202 srs2* is also suppressed by *top1* (Fig. 2a), including a complete loss of slippage events of 2 nucleotides and a reduction in single nucleotide slippage (Fig. 2b, Extended Data Table 1a).

The HU hypersensitivity (Fig. 2c), the hyper-rec phenotype (Fig. 2d), and the lethality with *pol2M644G* (Fig. 2e) of *rnh202 srs2* are also overcome by *top1*. Thus, when topoisomerase I is present, the tolerance of rNMPs needs RNaseH2 and Srs2, and recombinogenic DSBs arise when RNaseH2 is absent.

Topo I-mediated cleavage of a rNMP results in unligatable 5' hydroxyl and 3' cyclic phosphate termini²⁶. We reasoned that, in mutation avoidance, Srs2 unwinds DNA from the nick generated by Topo I. To test this, we constructed linear duplex DNA substrates whose ends are occluded by a Streptavidin-biotin complex. As expected, the intact substrate was resistant to unwinding by Srs2 (Extended Data Fig. 5). Importantly, when a nick bearing a 5' OH group was introduced, ATP-dependent displacement of the strand containing this group occurred (Extended Data Fig. 5). In contrast, little unwinding of the 3' OH bearing strand was seen (Extended Data Fig. 5).

To examine whether Srs2 unwinds DNA from a nick introduced by Topo I at an embedded ribonucleotide, a DNA substrate with a single UMP residue and blocked ends was prepared. As expected²⁶, calf thymus Topo I, but not *E. coli* Topo I, cleaved the DNA/rUMP hybrid strand, but not an equivalent substrate without the ribonucleotide (Extended Data Fig. 6a and 6b). Incubation of the Topo I-nicked DNA (Extended Data Fig. 6c) with Srs2 led to the ATP-dependent displacement of the strand with the 5' OH group, but not that contains the 3' cyclic phosphate (Fig. 3a). Mutations in *MPH1*, which encodes a 3'-5' helicase, also lead to a mutator phenotype²⁵. However, Mph1 protein does not act on the Topo I-nicked substrate (Extended Data Fig. 7a). Consistent with this, the *rnh202 mph1* double mutant shows the same dinucleotide slippage rate as *rnh202* (Extended Data Fig. 7b).

We surmised that Srs2-mediated unwinding of the 5'-strand at the Topo I-induced DNA nick prevents religation that is associated with DNA deletion and serves to initiate lesion removal by creating a DNA gap (see discussions later). If this were the case, one would expect a 5' endo- or exo- nuclease to be involved in the removal of the displaced DNA strand. One strong candidate is Exo1, which has 5' to 3' exonuclease and 5' FLAP endonuclease activities and plays a major role in DNA repair, including DNA break end resection during homologous recombination and DNA digestion during mismatch repair. Importantly, with the dinucleotide slippage reporter, we found that Exo1 has an antimutator activity against *rnh202*, and that it acts in an epistatic manner with Srs2 (Fig. 3b).

Being prompted by the genetic results, we next tested possible functional interactions between Srs2 and Exo1. For this, DNA substrates blocked at their ends and harbor a 5' FLAP or a 5' FLAP adjoining a gap were constructed; the latter substrate resembles the intermediate generated by Srs2-mediated DNA unwinding from a nick. We found that Exo1 acts endonucleolytically on these substrates, incising the single stranded arm of the FLAP structure (Extended Data Fig. 7c); little exonuclease activity was detected with these substrates or with an oligo dT substrate (Extended Data Fig. 7c). Importantly, Srs2 enhanced the endonucleolytic cleavage of the gapped 5'-FLAP DNA in an ATP-independent manner (Fig. 4a). Interestingly, by affinity pulldown, a physical interaction between Srs2 and Exo1 was detected (Fig. 4b). In contrast, we did not detect any enhancement of Exo1 activity by Mph1 (Extended Data Fig.8a). Moreover, although human EXO1 (hEXO1) digests the 5'

FLAP substrate similarly to yeast Exo1, addition of Srs2 led to inhibition of the reaction (Extended Data Fig. 8b). We also tested the effect of Srs2 on 5' FLAP cleavage mediated by yeast Dna2 and human FEN1 and found that Srs2 attenuates the cleavage efficiency in both cases (data not shown). These results support the premise that Srs2 and Exo1 co-operate, in a specific fashion, in the downstream processing of the DNA nick originating from Topo I-mediated cleavage at a rNMP.

hEXO1 can digest DNA exonucleolytically with 5'-3' polarity at a nick¹⁷, and we verified that yeast Exo1 has the same activity (Extended Data Fig. 7c). To ask how Exo1 processes different DNA nick types, we prepared substrates that harbor a Topo I-induced nick, a nick with 3' hydroxyl and 5' phosphate groups, or a nick with 3' and 5' hydroxyl groups. As shown in Fig. 4c, Exo1 can process the Topo I-induced nick, although less efficiently than it does a clean DNA nick. Interestingly, Srs2 enhanced digestion of the Topo I-induced nick, by as much as four fold (Fig. 4c (i) and (iv)). A stimulatory effect of Srs2, although less pronounced, on Exo1 was also observed with the nicked substrate harboring a 5'-OH group (Fig. 4c (ii) and (iv)), but little enhancement occurred at the nick that harbors 3' OH and 5' phosphate groups (Fig. 4c (iii) and (iv)). Again, ATP is dispensable for the observed stimulation (Fig. 4c), which suggests Srs2 facilitates the delivery of Exo1 to the cleaved rNMP site. We found that Mph1 is unable to stimulate Exo1-catalyzed digestion of the Topo I-induced nick (Extended Data Fig. 8c), and that digestion by hEXO1 is attenuated by Srs2 (Extended Data Fig. 8d).

The genetic and biochemical data presented above support the model (Extended Data Fig. 9) where Srs2 unwinds DNA from the Topo I-generated nick and recruits Exo1, which utilizes its 5' exonuclease or 5' FLAP endonuclease activity to generate a DNA gap to be filled by a DNA polymerase. In the absence of Srs2, unwinding of DNA from the 5' OH end is not possible and its processing by Exo1 also becomes inefficient. In this case, Topo I could act again at the 3' cyclic phosphate, cleaving two nucleotides and religating the ends to generate a two-nucleotide deletion¹⁵.

Recent evidence has suggested a beneficial role of DNA nicks stemming from ribonucleotide excision repair (RER) in the facilitation of DNA mismatch removal from the newly replicated DNA^{18,21}. However, rNMPs in DNA can be harmful, as they cause slippage and other mutations. To avoid such mutations, RNaseH2 initiates rNMP elimination via RER²⁸. We have shown that in the absence of RNaseH2, the major mechanism to remove embedded rNMPs is cleavage by Topo I and nick processing by Srs2/Exo1, followed by gap repair. rNMPs cleaved by Topo I may also be converted into a recombinogenic DSB. Our work thus uncovers a novel function of Srs2 helicase and Exo1 in mutation avoidance and rNMP lesion repair. Since the Srs2 helicase activity is required for the avoidance of rNMP-induced mutations, the major repair mechanism in cells may entail Srs2-mediated DNA strand separation from the Topo I-induced nick, to create a 5' FLAP for Exo1 to incise. The physical interaction between Srs2 and Exo1 likely serves to recruit the latter to the FLAP structure.

Methods Summary

Yeast strains are listed in Extended Data Table 1b

Mutation rates were determined by the Lea Coulson fluctuation method. Independent mutants were sequenced to identify mutations. Recombination assays were performed using the *leu2-ecoRI::URA3::leu2-bstEII* system as described¹⁰. For the (AG)₄ reporter, rates were determined as described^{8,29}. At least 18 independent cultures (minimum 2 isolates/genotype) were used to determine rates, and 95% confidence intervals were determined as described²⁹.

In vitro assays

Srs2 and Exo1 were expressed in *E. coli* and Hi5 insect cells, respectively, and purified as described^{12,27}. Purified hEXO1 was a gift from Guo-Min Li (University of Kentucky). Nuclease and helicase assays were conducted as described elsewhere; see Methods. Reactions were analyzed by gel electrophoresis and phosphorimaging.

Methods

In vivo assays

Yeast strains are listed in Extended Data Table 1b.

To determine mutation rates, *CAN1*⁺ strains were grown in 5 mL YPD overnight, washed and resuspended in 1 mL dH₂O. Cells were plated onto SC-arginine + 60 µg/mL canavanine to select for *can1* mutants and onto SC medium for total cell number. Plates were incubated at 30°C for 3–4 days. At least 18 independent cultures with a minimum of 2 different isolates per genotype were used to determine rates, calculated by the Lea and Coulson method of the median. 95% confidence intervals were determined as in²⁹. Independent mutants were sequenced at the *CAN1* locus to identify mutations. Recombination assays were performed using the *leu2-ecoRI::URA3::leu2-bstEII* system as described¹⁰. Briefly, colonies were struck out onto YPD medium and grown for 3 days at 30°C. Whole single colonies were resuspended in 1 mL dH₂O. Cells were plated to SC-leucine, -uracil to select for recombinants and onto SC medium for total cell number. Plates were incubated at 30°C for 3–4 days. At least 18 independent cultures with a minimum of 2 different isolates per genotype were used to determine rates, calculated by the Lea and Coulson method of the median. 95% confidence intervals were determined as in²⁹.

For the (AG)₄ reporter, rates were determined as described^{8,29}. Briefly, single colonies were inoculated into 5 mL YPD and grown for 2 days at 30°C, washed and resuspended in 1 mL dH₂O. Cells were plated onto SC-lysine medium to select for slippage mutants and onto SC medium for total cell number. Plates were incubated at 30°C for 3 days. At least 18 independent cultures with a minimum of 2 different isolates per genotype were used to determine rates, and 95% confidence intervals were determined as described²⁹.

DNA substrates

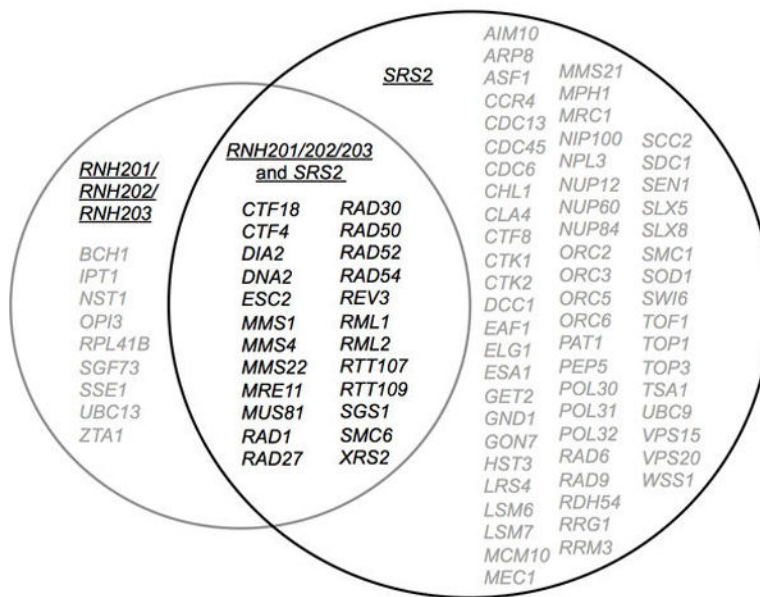
To construct the DNA substrates for helicase and nuclease assays, as diagramed in Extended Data Table 1c, selected oligonucleotides were first either 5' end-labeled with [γ - ^{32}P] ATP using T4 polynucleotide kinase (New England Biolab) or 3' end-labeled with [α - ^{32}P] Cordycepin 5'-triphosphate (PerkinElmer) and terminal deoxytransferase (Roche). The end-labeled oligonucleotides were then annealed to their partner oligonucleotides in buffer A (50 mM Tris-HCl, pH 7.5, 10 mM MgCl₂, 100 mM NaCl). The hybridized DNA substrates were further purified in a 10% native polyacrylamide gel followed by electroelution at 4°C. To introduce a nick at the rNMP site, the DNA duplex that contains a unique rUMP hybrid (50 pmol) was incubated with (60 units) calf thymus Topo I (Invitrogen) in the reaction buffer (50 mM Tris-HCl, pH 8.0, 50 mM KCl, 1 mM DTT) for 30 min at 37°C. After an incubation with SDS (0.2%) and proteinase K (0.5 mg/ml) for 10 min at 37°C, the DNA substrate was purified using a PCR cleaning kit (Qiagen).

Nuclease and helicase assays

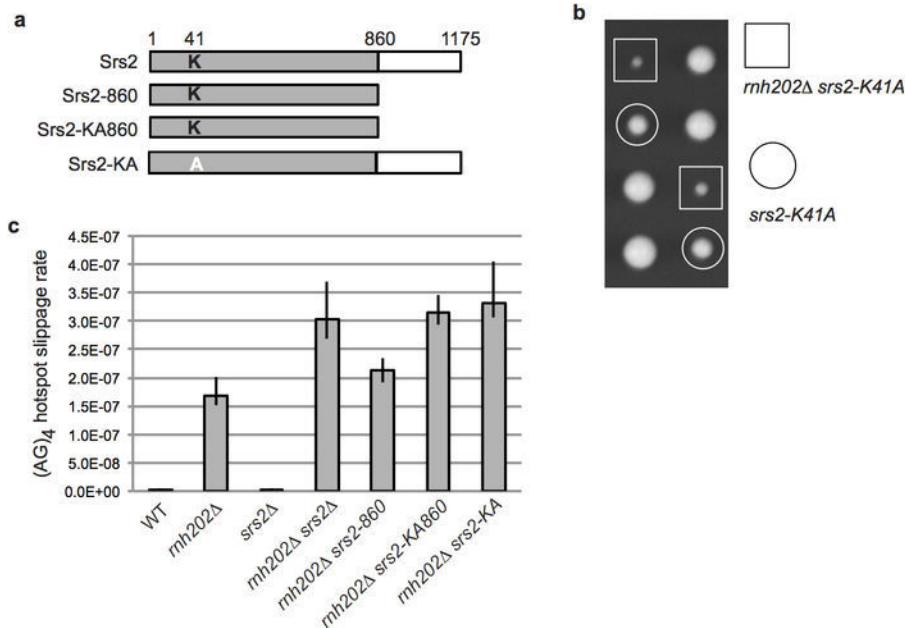
For nuclease assays, the DNA substrate (5 nM) was incubated with the indicated amount of Exo1 or hEXO1 in the reaction buffer (20 mM Tris-HCl, pH 7.5, 2 mM MgCl₂, 1 mM DTT, 200 ng / mL BSA, 50 mM KCl) for 10 min at 30°C or 37°C respectively. The reactions were fractionated in an 18% denaturing polyacrylamide gel followed by phosphorimaging analysis of the dried gel.

For helicase assays, the DNA substrate (5 nM) was incubated with the indicated amount of Srs2 or Mph1 in the reaction buffer (20 mM Tris-HCl, pH 7.5, 2 mM MgCl₂, 1 mM DTT, 200 ng / mL BSA, 50 mM KCl) with 1 mM ATP and the ATP regenerating system for 10 min at 30°C. The reactions were fractionated in a 12% native polyacrylamide gel followed by phosphorimaging analysis of the dried gel.

Extended Data

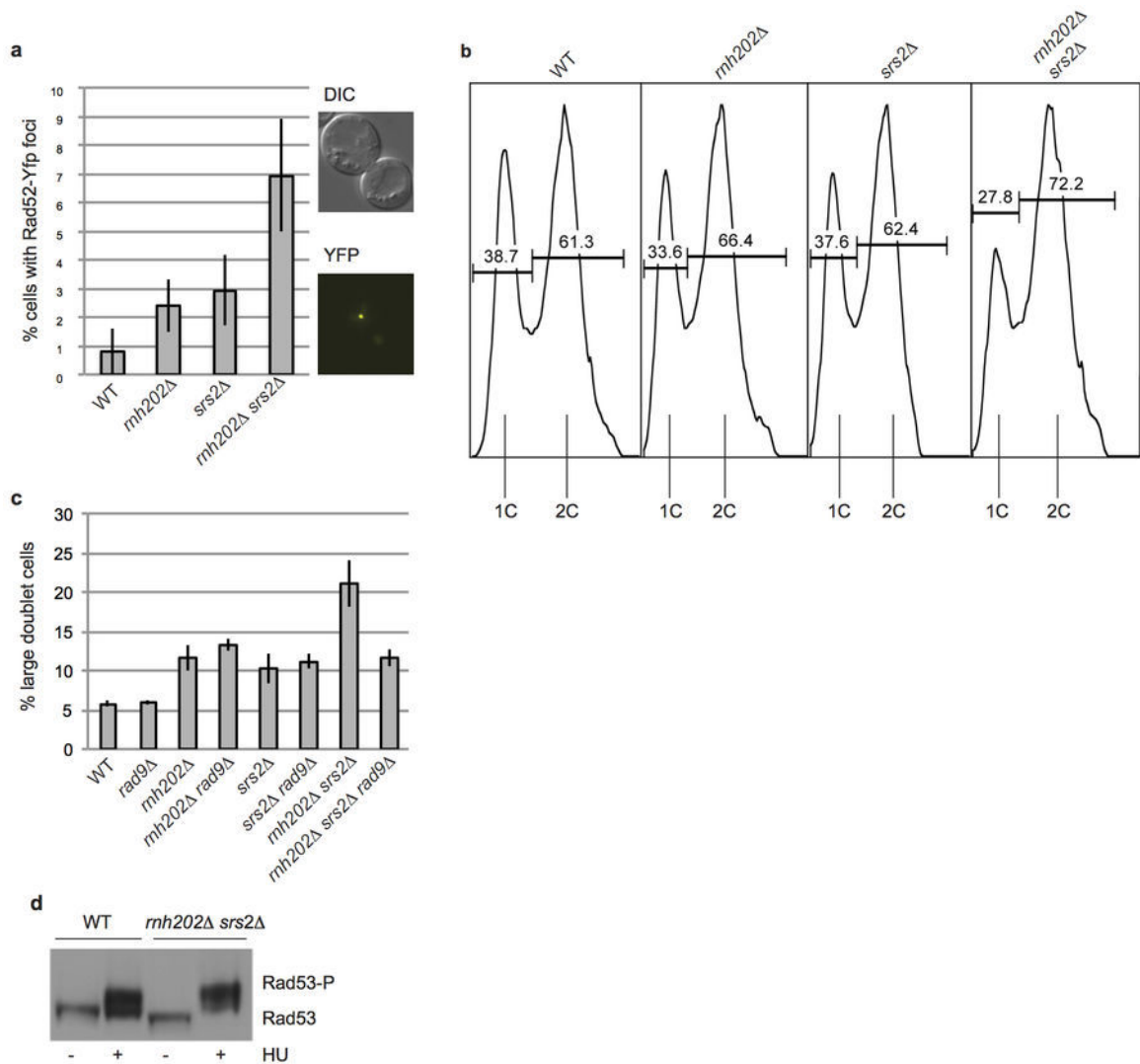


Extended Data Figure 1. Genetic interactions of the *RNH201/202/203* genes and *SRS2*
 Lists of genes were obtained from the Saccharomyces Genome Database. Genes in grey are synthetically sick or synthetically lethal with either *RNH201/RNH202/RNH203* or with *SRS2*. Genes in black are synthetically sick/lethal with both *RNH201/RNH202/RNH203* and *SRS2*.



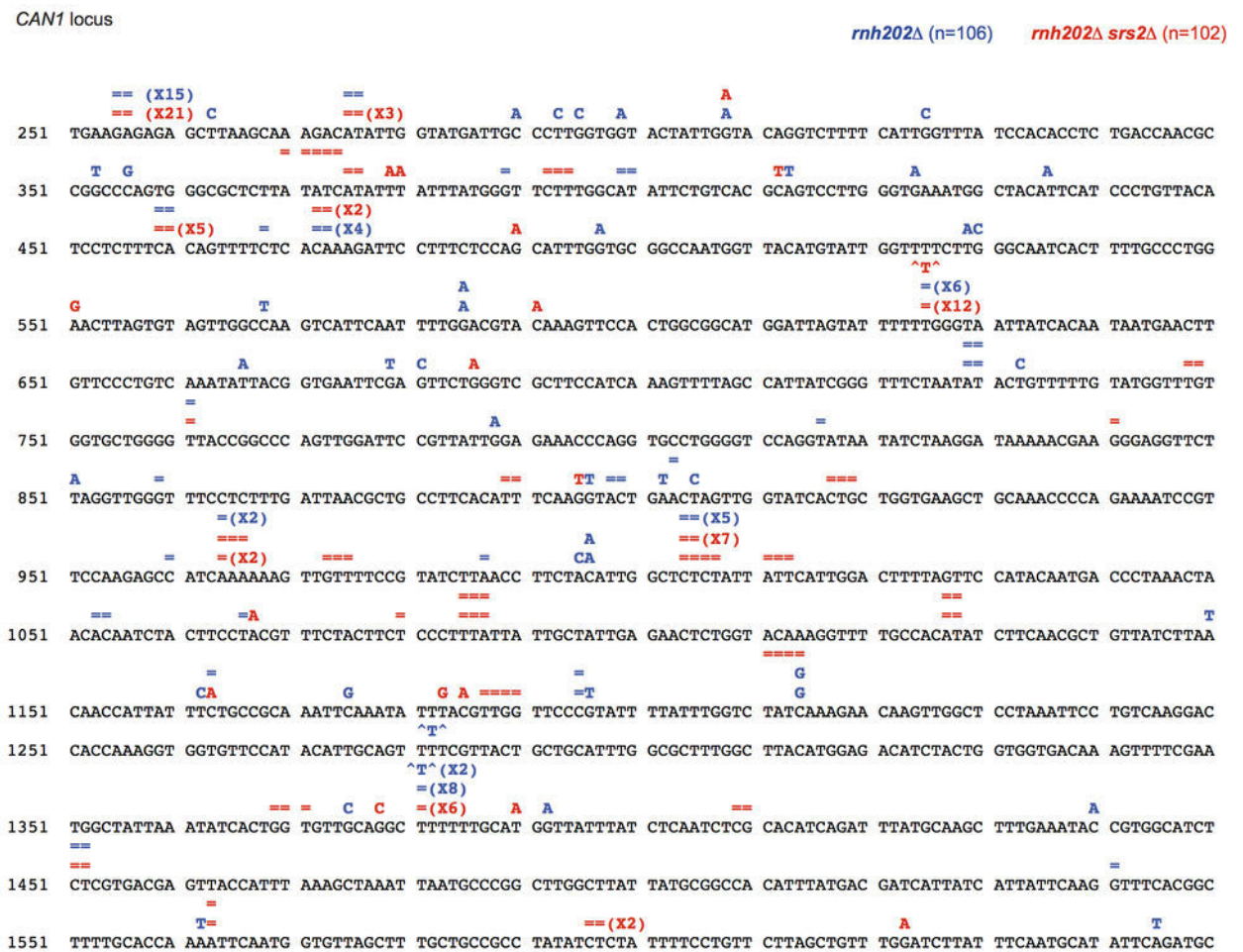
Extended Data Figure 2. Full-length *srs2-KA* displays the same double mutant phenotype with *rnh202* as do *srs2* and *srs2-KA860*

a. Strains harboring the helicase null K41A variant at the chromosomal *SRS2* locus were constructed. **b.** Synthetic interaction of *rmh202* and *srs2-KA*. **c.** Dinucleotide slippage rates; plotted are median rates with error bars representing 95% confidence intervals²⁹; n=18.



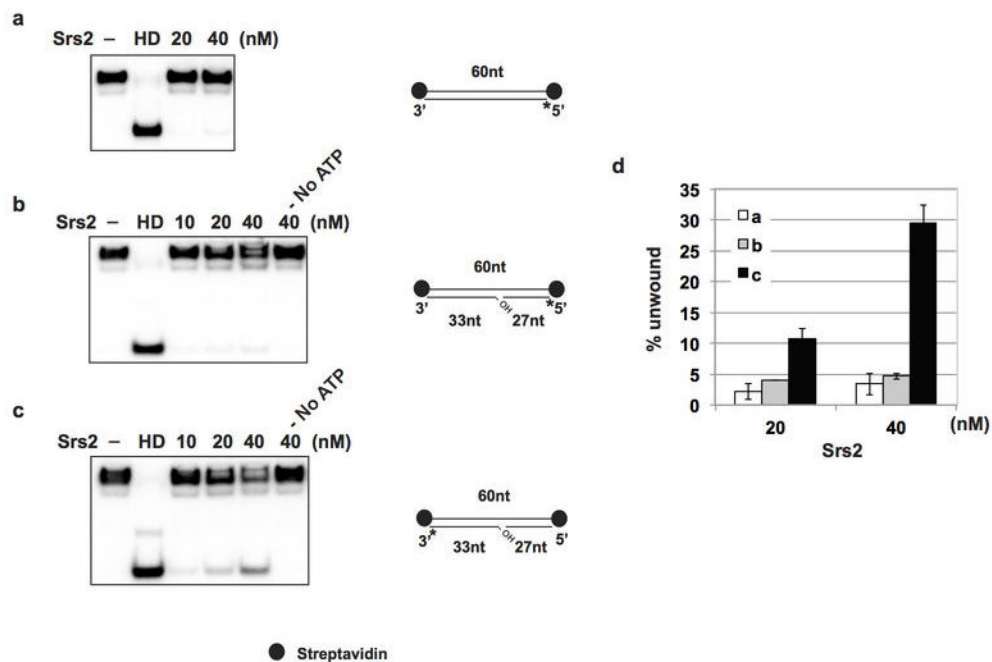
Extended Data Figure 3. Increased DNA damage load in the *rmh202 srs2* double mutant

a. Left, percentage cells with spontaneous Rad52-Yfp foci formation, with at least 10 fields of 50–200 cells counted per strain. Right, representative DIC and YFP images of a Rad52-Yfp focus. **b.** Log phase cells were analyzed by flow cytometry to determine DNA content and data were quantified using FlowJo software. **c.** Percentage of large doublet cells in mid-log phase cultures. Total number of cells and number of large doublet cells were determined for each strain by examining at least 10 fields of 50–200 cells per strain. **d.** Wild type and *rmh202 srs2* double mutant cells were grown in YPD media, washed and treated for 1 hour with 100 mM HU. Lysates were extracted and subjected to immunoblotting with an anti-Rad53 antibody¹⁶. The higher species represents phosphorylated Rad53. Plotted in (a) and (c) are the mean values \pm s.d, n=3.



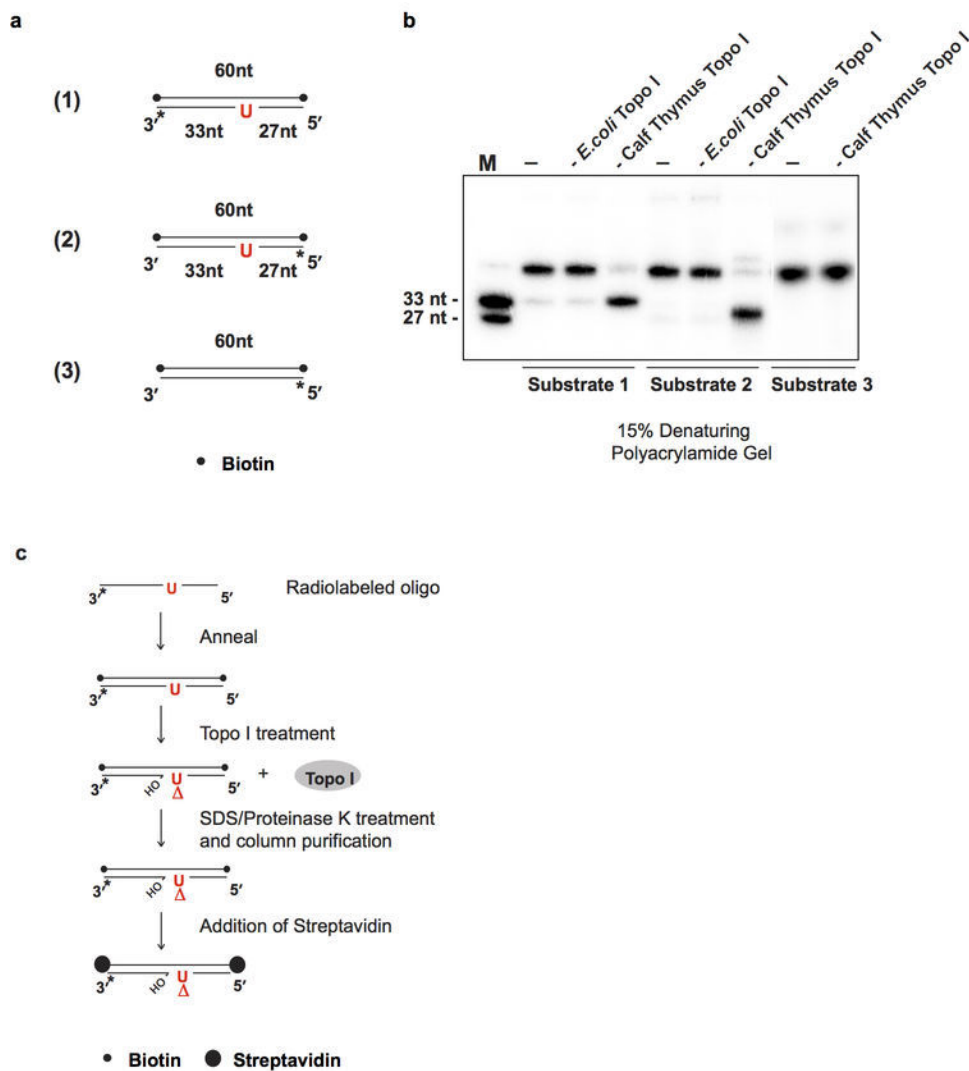
Extended Data Figure 4. Mutation spectra at the *CAN1* locus for the *rnh202* single and *rnh202 srs2* double mutant cells

Independent mutations in the *rnh202* (in blue) and *rnh202 srs2* (in red) *Can^R* mutant strains. Base substitutions are written above the wild type sequence, deletions are represented by “=”, and insertions are represented by “^N^”.



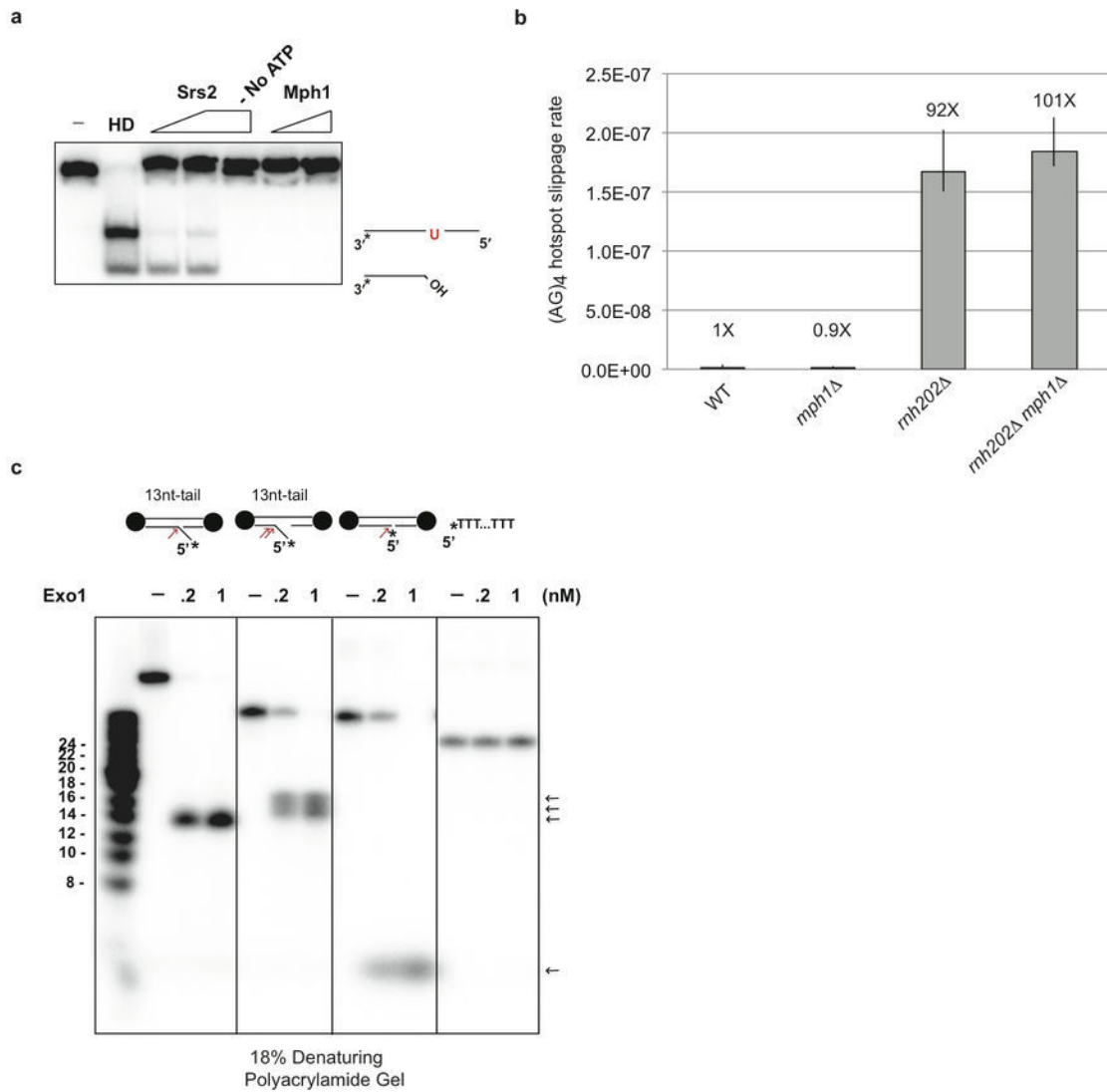
Extended Data Figure 5. Unwinding of nicked duplex DNA by Srs2

Intact duplex DNA (**a**) and nicked duplex DNA labeled at either the 5' end (**b**) or the 3' end (**c**) of the nicked strand were incubated with Srs2 for 10 min at 30°C with or without ATP. Reactions were run in a polyacrylamide gel and analyzed by phosphorimaging analysis. The results were quantified in (**d**). Plotted are the mean values \pm s.d, $n=3$.



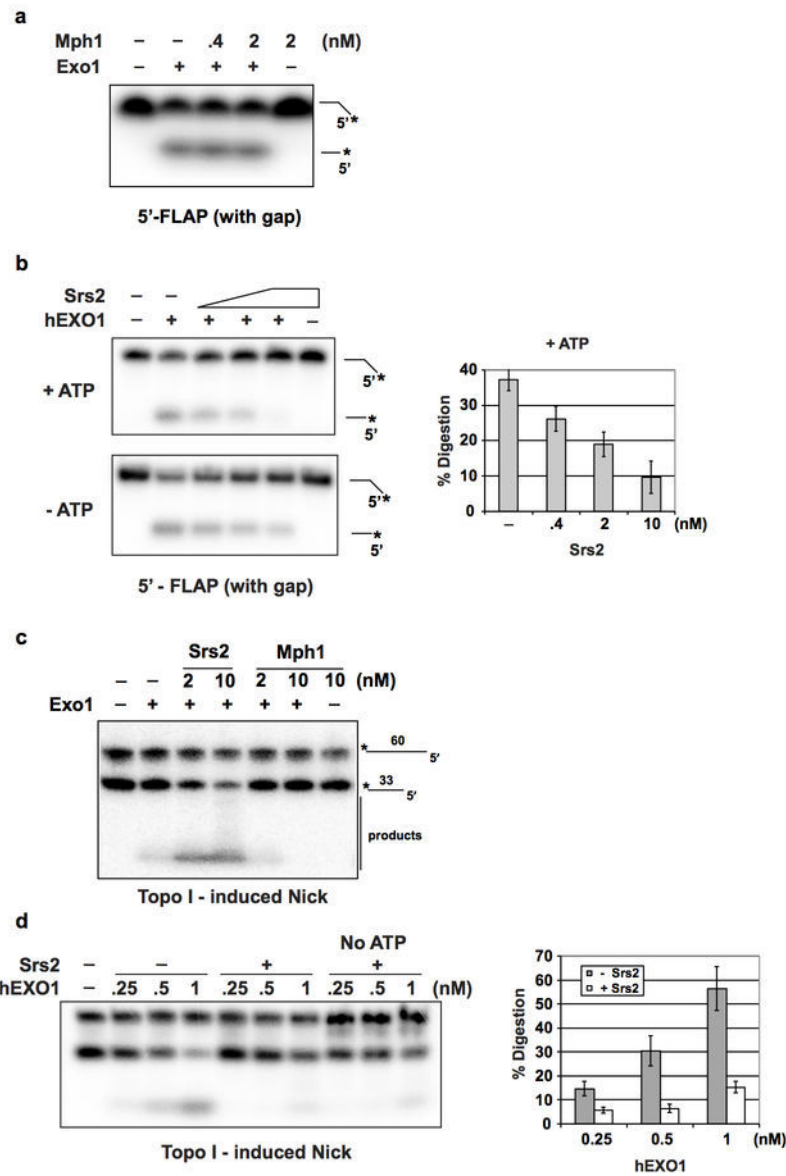
Extended Data Figure 6. Topo I-catalyzed DNA cleavage at the rUMP site

Duplex DNA with or without an embedded rUMP residue (5 nM) (a) were incubated with either *E. coli* or Calf thymus Topo I for 30 min at 37°C. Reactions were analyzed by electrophoresis in a polyacrylamide gel followed by phosphorimaging analysis (b). A schematic for the construction of the DNA substrate that harbors a unique nick induced by calf thymus Topo I at a rUMP residue (c).



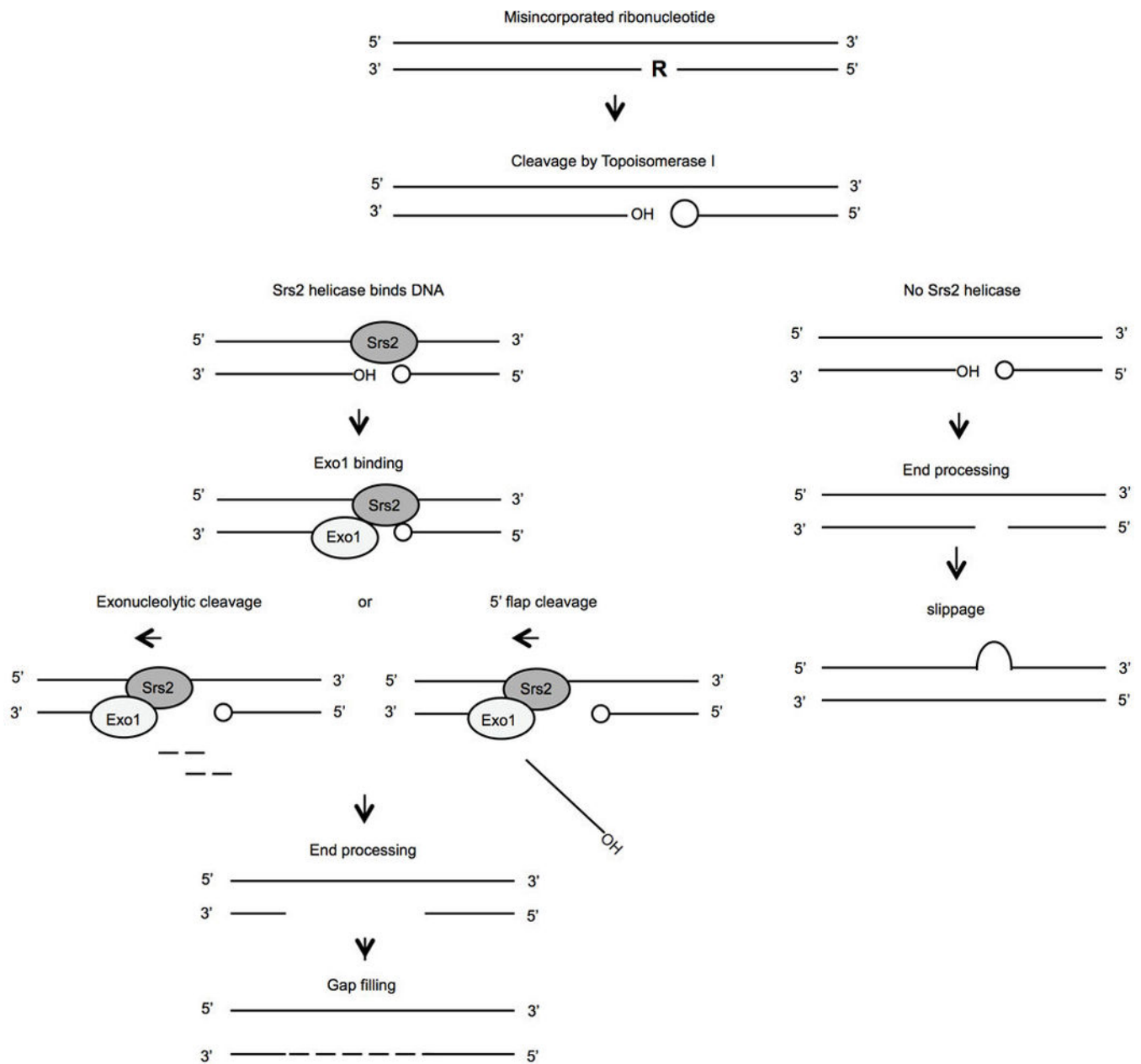
Extended Data Figure 7. Mph1 does not act at the Topo I –induced nick

a. DNA substrate (5 nM) that harbors a Topo I-induced nick and radiolabeled on the 3' side was incubated with Srs2 or Mph1 (20 or 40 nM) in the presence or absence of ATP at 30°C for 10 min. The reactions were analyzed as before. **b.** (AG)₄ dinucleotide slippage rates; plotted are median rates with error bars representing 95% confidence intervals²⁹; n=18 **c.** **Exo1 displays 5' endo- and exo- nuclease activities on the 5'-FLAP and the nicked duplex DNA, respectively.** Radiolabeled 5'-FLAP without or with a gap region, nicked duplex DNA, or oligo dT (5 nM each) was incubated with Exo1 for 10 min at 30°C. The reactions were analyzed as before and the products indicated by the arrows.



Extended Data Figure 8. Stimulation of Exo1-catalyzed digestion of a 5'-FLAP and a Topo I-induced nick by Srs2

a. Radiolabeled 5'-FLAP substrate (5 nM) was incubated with Exo1 (0.1 nM) in the absence or presence of Mph1 for 10 min at 30°C. **b.** The radiolabeled 5'-FLAP substrate (5 nM) was incubated with hEXO1 (4 nM) in the absence or presence of Srs2 (0.4, 2 and 10 nM) for 10 min at 37°C. **c.** Radiolabeled DNA substrate harboring a Topo I-induced nick (5 nM) was incubated with Exo1 (0.1 nM) in the absence or presence of Srs2 or Mph1 for 10 min at 30°C. **d.** The radiolabeled substrate harboring a Topo I-induced nick (5 nM) was incubated with increasing amounts of hEXO1 (0.25, 0.5 and 1 nM) in the absence or presence of Srs2 (10 nM) for 10 min at 37°C. The reactions in (a), (b), (c) and (d) were analyzed as before. Plotted in (b) and (d) are the mean values \pm s.d, n=3.



Extended Data Figure 9. Model of Srs2/Exo1-mediated processing of a DNA nick induced by Top1 at an embedded ribonucleotide

RNase H2 normally removes misincorporated rNMPs from DNA (not shown). In the absence of RNase H2, topoisomerase 1 can cleave at the embedded ribonucleotide, leaving 3' cyclic phosphate and 5' OH ends that cannot be ligated. Repair commences with unwinding of DNA from the 5' OH side by Srs2, followed by DNA digestion by Exo1 via its exonuclease or 5' FLAP endonuclease activity to result in a DNA gap, to be filled by a DNA polymerase. Our results show that Srs2 enhances the nuclease activities of Exo1. In the absence of Srs2, religation of ends processed by unknown nuclease activities leads to a deletion mutation.

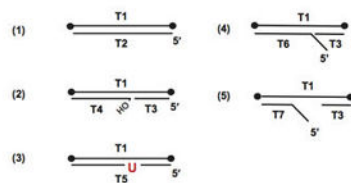
Extended Data Table 1

a. Can^r mutation spectra. b. Yeast Strains c. Sequences of oligo nucleotides used.

	Total	Base change	1 nt repeat	≥2 nt repeat
WT	52	52	0	0
<i>mh202Δ</i>	106	41	33	32
<i>srs2Δ</i>	61	48	8	5
<i>mh202Δ srs2Δ</i>	102	16	27	59
<i>mh202Δ top1Δ</i>	54	40	14	0
<i>mh202Δ srs2Δ top1Δ</i>	50	33	17	0

b	
579-10D	<i>MATa ade2-1 can1-100 his3-11,15 leu2-3,112 trp1-1 ura3-1</i>
2190	<i>mh202::KANMX4 MATa</i>
590-6D	<i>srs2::HIS3 MATa ade2-1</i>
2281-9D	<i>mh202::KANMX4 srs2::HIS3 MATa</i>
2070-4	<i>srs2-860::HPHMX MATa</i>
2484	<i>srs2-KA860::HPHMX MATa</i>
2420-2B	<i>mh202::KANMX4 srs2-860::HPHMX MATa</i>
2482-2A	<i>mh202::KANMX4 srs2-KA860::HPHMX MATa</i>
1093-5A	<i>MATa CAN1</i>
2359-7C	<i>mh202::KANMX4 MATa CAN1</i>
1307-1B	<i>srs2::HIS3 MATa CAN1</i>
2358-11B	<i>mh202::KANMX4 srs2::HIS3 MATa</i>
2442-1C	<i>srs2-860::HPHMX MATa CAN1</i>
2556-4B	<i>srs2-KA860::HPHMX MATa CAN1</i>
2442-3B	<i>mh202::KANMX4 srs2-860::HPHMX MATa</i>
2556-8D	<i>mh202::KANMX4 srs2-KA860::HPHMX MATa</i>
660-2A	<i>leu2-EcoRI::URA3-leu2-BstEII MATa</i>
2191	<i>mh202::KANMX4 leu2-EcoRI::URA3-leu2-BstEII MATa</i>
1323-1B	<i>srs2::HIS3 leu2-EcoRI::URA3-leu2-BstEII MATa</i>
100-3C	<i>mh202::KANMX4 srs2::HIS3 leu2-EcoRI::URA3-leu2-BstEII MATa</i>
200-3D	<i>lys2ΔA746NR,(AG)_n MATa</i>
201-7D	<i>mh202::KANMX4 lys2ΔA746NR,(AG)_n MATa</i>
202-6C	<i>srs2::HIS3 lys2ΔA746NR,(AG)_n MATa</i>
203-5B	<i>mh202::KANMX4 srs2::HIS3 lys2ΔA746NR,(AG)_n MATa</i>
2769-5B	<i>mh202::KANMX4 srs2-860::HPHMX lys2ΔA746NR,(AG)_n MATa</i>
2746-1B	<i>mh202::KANMX4 srs2-KA860::HPHMX lys2ΔA746NR,(AG)_n MATa</i>
2470-5A	<i>top1::HPHMX MATa ade2-1</i>
2470-1C	<i>mh202::KANMX4 top1::HPHMX MATa</i>
2470-1B	<i>srs2::HIS3 top1::HPHMX MATa</i>
2470-5B	<i>mh202::KANMX4 srs2::HIS3 top1::HPHMX MATa</i>
2529-8D	<i>top1::HPHMX MATa ade2-1 CAN1</i>
2529-3D	<i>mh202::KANMX4 top1::HPHMX MATa</i>
2529-10C	<i>srs2::HIS3 top1::HPHMX MATa ade2-1 CAN1</i>
2529-4B	<i>mh202::KANMX4 srs2::HIS3 top1::HPHMX MATa</i>
2501-11A	<i>top1::HPHMX leu2-EcoRI::URA3-leu2-BstEII MATa</i>
2477-1C	<i>mh202::KANMX4 top1::HPHMX leu2-EcoRI::URA3-leu2-BstEII MATa</i>
2501-2A	<i>srs2::HIS3 top1::HPHMX leu2-EcoRI::URA3-leu2-BstEII MATa</i>
2477-1B	<i>mh202::KANMX4 srs2::HIS3 top1::HPHMX leu2-EcoRI::URA3-leu2-BstEII MATa</i>
2828-17C	<i>mre11-H125N::URA3 MATa CAN1</i>
2828-5A	<i>mh202::KANMX4 mre11-H125N::URA3 MATa CAN1</i>
2828-22C	<i>srs2::HIS3 mre11-H125N::URA3 MATa CAN1</i>
2828-10A	<i>mh202::KANMX4 srs2::HIS3 mre11-H125N::URA3 MATa CAN1</i>
2869	<i>MATa pol2M644G</i>
3050-4B	<i>mh202::KANMX4 mph1::KANMX4 lys2ΔA746NR,(AG)_n MATa</i>
3050-1C	<i>mph1::KANMX4 lys2ΔA746NR,(AG)_n MATa</i>
2894-9C	<i>mh202::KANMX4 srs2::HIS3 exo1::URA3 lys2ΔA746NR,(AG)_n MATa</i>
2894-10A	<i>mh202::KANMX4 exo1::URA3 lys2ΔA746NR,(AG)_n MATa</i>
2894-1D	<i>srs2::HIS3 exo1::URA3 lys2ΔA746NR,(AG)_n MATa</i>
2894-4C	<i>exo1::URA3 lys2ΔA746NR,(AG)_n MATa</i>
3132-4D	<i>mh202::KANMX4 srs2-K41A_lys2ΔA746NR,(AG)_n MATa</i>

c	
T1	biotin - GCAAGCAGAAGCCAGACAAAGGTTTGGCCACATATCTTCAACGCTCGAACGTCGGAACCG - biotin
T2	CGGTTCCGACGTTCCGAGCGTTGAAGATATGTGGCAAACCTTTGTCTGGCTTCTGCTTGC
T3	CGGTTCCGACGTTCCGAGCGTTGAAGAT
T4	ATGTGGCAAACCTTTGTCTGGCTTCTGCTTGC
T5	CGGTTCCGACGTTCCGAGCGTTGAAGAJATGTGGCAAACCTTTGTCTGGCTTCTGCTTGC
T6	TTTTTTTTTTTTATGTGGCAAACCTTTGTCTGGCTTCTGCTTGC
T7	TTTTTTTTTTTTTTTGTCTGGCTTCTGCTTGC



Acknowledgments

We thank S. Jinks-Robertson and T. Kunkel for plasmids used in strain construction, R. Bermejo and M. Foiani for the genome sequencing of the original *hpr4* strain, and Guo-Min Li and Sanghee Lee for providing hEXO1. This work was supported by NIH grants RO1GM053738 (HLK), RO1ES007061 (PS), and K99ES021441 (HN).

References

- Colavito S, et al. Functional significance of the Rad51-Srs2 complex in Rad51 presynaptic filament disruption. *Nucleic acids research*. 2009; 37:6754–6764.10.1093/nar/gkp748 [PubMed: 19745052]
- Krejci L, et al. DNA helicase Srs2 disrupts the Rad51 presynaptic filament. *Nature*. 2003; 423:305–309.10.1038/nature01577 [PubMed: 12748644]
- Van Komen S, Reddy MS, Krejci L, Klein H, Sung P. ATPase and DNA helicase activities of the *Saccharomyces cerevisiae* anti-recombinase Srs2. *The Journal of biological chemistry*. 2003; 278:44331–44337.10.1074/jbc.M307256200 [PubMed: 12966095]
- Aboussekhra A, Chanet R, Adjiri A, Fabre F. Semidominant suppressors of Srs2 helicase mutations of *Saccharomyces cerevisiae* map in the RAD51 gene, whose sequence predicts a protein with similarities to procaryotic RecA proteins. *Molecular and cellular biology*. 1992; 12:3224–3234. [PubMed: 1620127]
- Chanet R, Heude M, Adjiri A, Maloisel L, Fabre F. Semidominant mutations in the yeast Rad51 protein and their relationships with the Srs2 helicase. *Molecular and cellular biology*. 1996; 16:4782–4789. [PubMed: 8756636]
- Veaute X, et al. The Srs2 helicase prevents recombination by disrupting Rad51 nucleoprotein filaments. *Nature*. 2003; 423:309–312.10.1038/nature01585 [PubMed: 12748645]
- Bhattacharyya S, Lahue RS. *Saccharomyces cerevisiae* Srs2 DNA helicase selectively blocks expansions of trinucleotide repeats. *Molecular and cellular biology*. 2004; 24:7324–7330.10.1128/MCB.24.17.7324-7330.2004 [PubMed: 15314145]
- Kim N, et al. Mutagenic processing of ribonucleotides in DNA by yeast topoisomerase I. *Science*. 2011; 332:1561–1564.10.1126/science.1205016 [PubMed: 21700875]
- Crow YJ, et al. Mutations in genes encoding ribonuclease H2 subunits cause Aicardi-Goutieres syndrome and mimic congenital viral brain infection. *Nature genetics*. 2006; 38:910–916.10.1038/ng1842 [PubMed: 16845400]
- Aguilera A, Klein HL. Genetic control of intrachromosomal recombination in *Saccharomyces cerevisiae*. I. Isolation and genetic characterization of hyper-recombination mutations. *Genetics*. 1988; 119:779–790. [PubMed: 3044923]
- Krejci L, et al. Role of ATP hydrolysis in the antirecombinase function of *Saccharomyces cerevisiae* Srs2 protein. *The Journal of biological chemistry*. 2004; 279:23193–23199.10.1074/jbc.M402586200 [PubMed: 15047689]
- Adkins NL, Niu H, Sung P, Peterson CL. Nucleosome dynamics regulates DNA processing. *Nat Struct Mol Biol*. 2013; 20:836–842.10.1038/nsmb.2585 [PubMed: 23728291]
- Burgess RC, et al. Localization of recombination proteins and Srs2 reveals anti-recombinase function in vivo. *J Cell Biol*. 2009; 185:969–981.10.1083/jcb.200810055 [PubMed: 19506039]
- Chen C, Umezu K, Kolodner RD. Chromosomal rearrangements occur in *S. cerevisiae* *rfal* mutator mutants due to mutagenic lesions processed by double-strand-break repair. *Molecular cell*. 1998; 2:9–22. [PubMed: 9702187]
- Cho JE, Kim N, Li YC, Jinks-Robertson S. Two distinct mechanisms of Topoisomerase 1-dependent mutagenesis in yeast. *DNA repair*. 2013; 12:205–211.10.1016/j.dnarep.2012.12.004 [PubMed: 23305949]
- Fiorani S, Mimun G, Caleca L, Piccini D, Pellicoli A. Characterization of the activation domain of the Rad53 checkpoint kinase. *Cell Cycle*. 2008; 7:493–499. [PubMed: 18287812]
- Genschel J, Bazemore LR, Modrich P. Human exonuclease I is required for 5' and 3' mismatch repair. *The Journal of biological chemistry*. 2002; 277:13302–13311.10.1074/jbc.M111854200 [PubMed: 11809771]

18. Ghodgaonkar MM, et al. Ribonucleotides misincorporated into DNA act as strand-discrimination signals in eukaryotic mismatch repair. *Molecular cell*. 2013; 50:323–332.10.1016/j.molcel.2013.03.019 [PubMed: 23603115]
19. Lee Bi BI, Nguyen LH, Barsky D, Fernandes M, Wilson DM 3rd. Molecular interactions of human Exo1 with DNA. *Nucleic acids research*. 2002; 30:942–949. [PubMed: 11842105]
20. Lisby M, Rothstein R, Mortensen UH. Rad52 forms DNA repair and recombination centers during S phase. *Proceedings of the National Academy of Sciences of the United States of America*. 2001; 98:8276–8282.10.1073/pnas.121006298 [PubMed: 11459964]
21. Lujan SA, Williams JS, Clausen AR, Clark AB, Kunkel TA. Ribonucleotides are signals for mismatch repair of leading-strand replication errors. *Molecular cell*. 2013; 50:437–443.10.1016/j.molcel.2013.03.017 [PubMed: 23603118]
22. Macris MA, Sung P. Multifaceted role of the *Saccharomyces cerevisiae* Srs2 helicase in homologous recombination regulation. *Biochemical Society transactions*. 2005; 33:1447–1450.10.1042/BST20051447 [PubMed: 16246143]
23. Nick McElhinny SA, et al. Genome instability due to ribonucleotide incorporation into DNA. *Nature chemical biology*. 2010; 6:774–781.10.1038/nchembio.424 [PubMed: 20729855]
24. Nick McElhinny SA, et al. Abundant ribonucleotide incorporation into DNA by yeast replicative polymerases. *Proceedings of the National Academy of Sciences of the United States of America*. 2010; 107:4949–4954.10.1073/pnas.0914857107 [PubMed: 20194773]
25. Scheller J, Schurer A, Rudolph C, Hettwer S, Kramer W. MPH1, a yeast gene encoding a DEAH protein, plays a role in protection of the genome from spontaneous and chemically induced damage. *Genetics*. 2000; 155:1069–1081. [PubMed: 10880470]
26. Sekiguchi J, Shuman S. Site-specific ribonuclease activity of eukaryotic DNA topoisomerase I. *Molecular cell*. 1997; 1:89–97. [PubMed: 9659906]
27. Seong C, Colavito S, Kwon Y, Sung P, Krejci L. Regulation of Rad51 recombinase presynaptic filament assembly via interactions with the Rad52 mediator and the Srs2 anti-recombinase. *The Journal of biological chemistry*. 2009; 284:24363–24371.10.1074/jbc.M109.032953 [PubMed: 19605344]
28. Sparks JL, et al. RNase H2-initiated ribonucleotide excision repair. *Molecular cell*. 2012; 47:980–986.10.1016/j.molcel.2012.06.035 [PubMed: 22864116]
29. Spell RM, Jinks-Robertson S. Determination of mitotic recombination rates by fluctuation analysis in *Saccharomyces cerevisiae*. *Methods Mol Biol*. 2004; 262:3–12.10.1385/1-59259-761-0:003 [PubMed: 14769952]

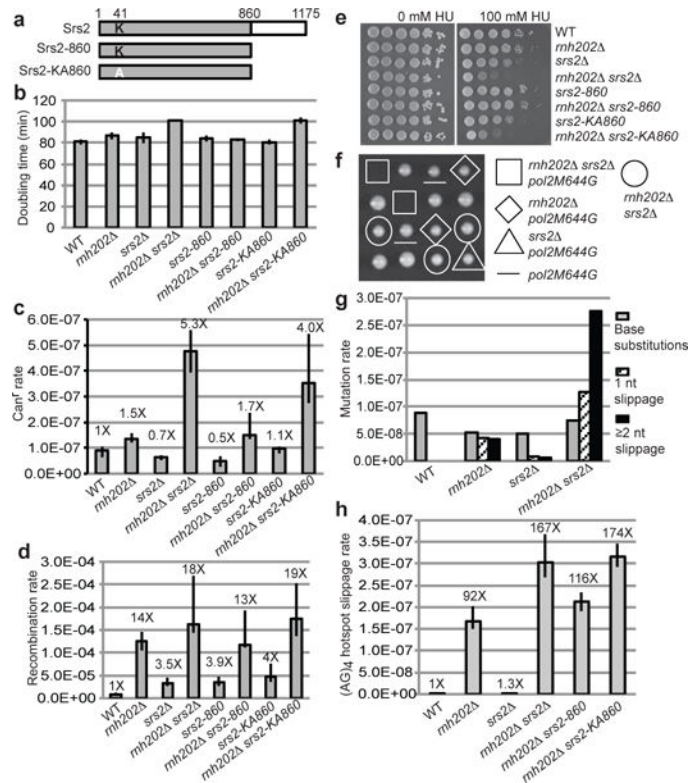


Figure 1. Genome stability maintenance role of Srs2 helicase in *rnh202* cells

a. Strains harboring either the *srs2-860* allele or its helicase null K41A variant at the chromosomal *SRS2* locus were constructed. **b.** Doubling times. **c.** Spontaneous mutation rates. **d.** Recombination rates. **e.** Sensitivity to hydroxyurea (HU). **f.** Synthetic interaction of the *pol2M644G* mutation in the *rnh202 srs2* background. **g.** Mutation spectra of Can^R mutants obtained in (c). **h.** Dinucleotide slippage rates. Plotted in (b) are the mean values \pm s.d., n=3. Plotted in (c), (d) and (h) are median rates with error bars representing 95% confidence intervals²⁹; n=18.

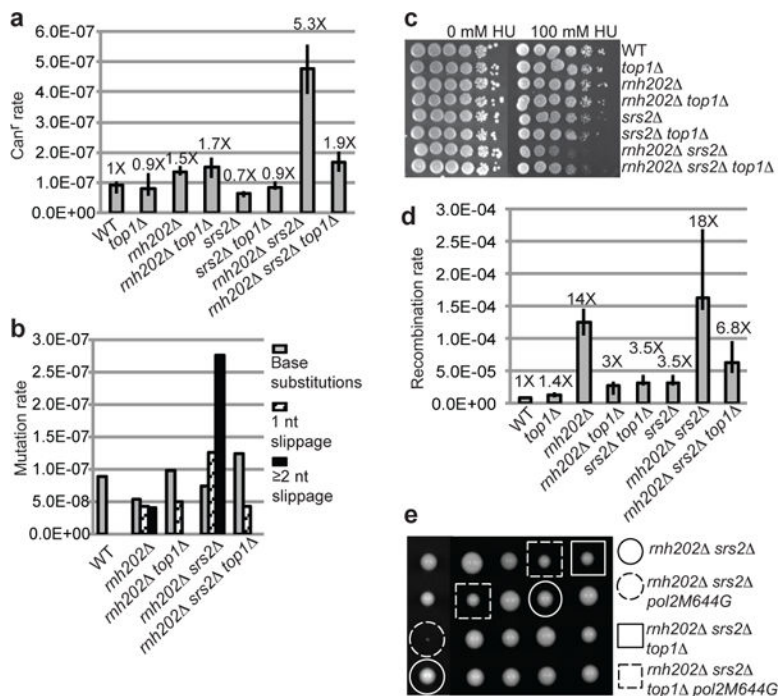


Figure 2. Causation of genome instability in *rnh202 srs2* mutant by Top1

a. Spontaneous mutation rates. **b.** Mutation spectra of Can^r mutants obtained in (a). **c.** Sensitivity to hydroxyurea (HU). **d.** Recombination rates. **e.** Synthetic interaction of the *pol2M644G* mutation in the *rnh202 srs2 top1* background. Plotted in (a) and (d) are median rates with error bars representing 95% confidence intervals²⁹; n=18.

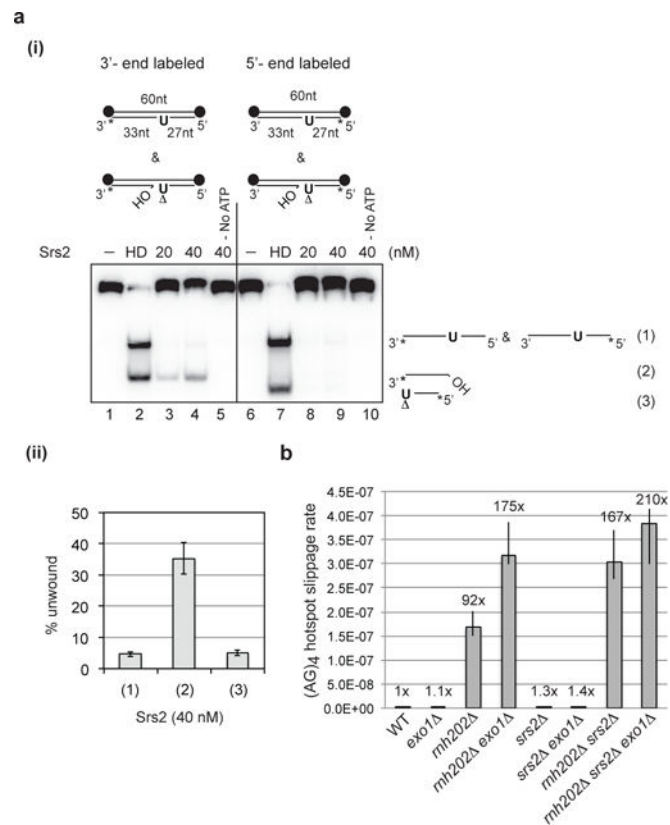


Figure 3. a. Srs2-mediated displacement of the 5'-strand at a Topo I-induced DNA nick DNA substrates containing a Topo I-induced nick and labeled at either the 3' or 5' end were incubated with Srs2 with or without ATP. The reactions were analyzed on a polyacrylamide gel (i); the results were quantified (ii). Heat-denatured (HD) DNA was analyzed in lanes 2 and 7. **b. Effects of Exo1 deletion on slippage mutations in *rnh202* and *rnh202 srs2* mutant cells.** Dinucleotide slippage rates. Plotted in (a) are the mean values \pm s.d., $n=3$; in (b), median rates with error bars representing 95% confidence intervals²⁹; $n=18$.

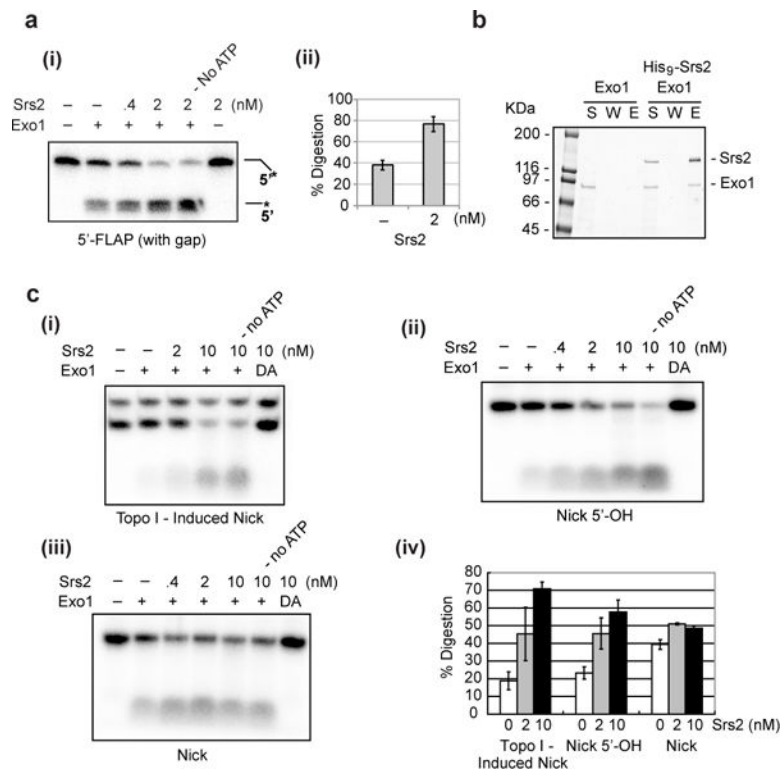


Figure 4. Interactions of Exo1 with Srs2

a. Endonucleolytic cleavage of a gapped 5'-FLAP DNA by Exo1 (0.1 nM) was examined with and without Srs2 or ATP. The reactions were analyzed on a polyacrylamide gel **(i)** and the results were quantified **(ii)**. **b.** Affinity pulldown through the (His)₉ tag on Srs2 was used to analyze its interaction with Exo1. The supernatant (S), wash (W) and SDS eluate (E) fractions were analyzed by 4–20% SDS-PAGE. **c.** Exonucleolytic cleavage of a **(i)** Topo I-induced nick, **(ii)** nick bearing a 5'-OH group, and **(iii)** clean nick bearing a 5'-phosphate by Exo1 was examined with and without Srs2 or ATP. The reactions were analyzed as above **(iv)**. Plotted in (a) and (c) are the mean values \pm s.d., n=3.